

Revealing the Role of Methylammonium Iodide Purity on the Vapor-Phase Deposition Process of Perovskites

Marcel Roß,* Marvin B. Stutz, and Steve Albrecht*

Vapor deposition processes, well established in the industry, are considered a cost-effective manufacturing route for large-area depositions of lead halide perovskites. However, the vapor deposition of perovskites is constrained by its low reproducibility, whereby in particular the evaporation of methylammonium iodide (MAI) is frequently reported as extremely challenging. Herein, the influence of impurities on the evaporation dynamics of MAI is analyzed. It is proved that MAI heated in a high vacuum, depending on the purity, either undergoes a sublimation with a subsequent desublimation or a chemical decomposition with a following reverse reaction, leading to solid MAI in both cases. In situ mass spectrometry enables us to show that low purity MAI containing water and methylammonium phosphite impurities mainly sublimates, which results in a directional and by crystal microbalances traceable evaporation. In contrast, high purity MAI sublimates at higher temperatures and tends to form decomposition products such as methylamine and hydrogen iodide, which omnidirectional diffuse and can react with lead iodide to perovskite. The findings reveal the reason for the reported challenges, serve as a guideline for future material selections, and can enhance the reproducibility of the evaporation process to achieve a more controlled solar cell fabrication.

1. Introduction

Lead halide perovskites are promising candidates for optoelectronic applications, as they combine a high absorption

coefficient, a steep absorption onset, and a certain tolerance against defects with low-cost favorable manufacturing perspectives.^[1–4] In particular, the rapid rise in perovskite solar cell efficiency from below 10% to over 25% in less than 10 years attracted international attention.^[5,6]


Currently, high-efficiency perovskite solar cells (PSCs) are typically prepared by solution-based processes, although evaporation techniques, which are widely used in the semiconductor industry, offer unique advantages.^[7,8] In particular, vacuum processes enable the deposition of very smooth films and provide excellent control over film thickness and composition.^[9] In addition, up-scaling to larger areas is feasible once the process control is realized. To monitor the evaporation process, quartz crystal microbalances (QCM) are commonly used.^[7,10] Although the co-evaporation process for perovskites was already successfully demonstrated in 2013^[11] and recently enabled solar cell efficiencies of over 20%,^[12–14] the imple-

mentation of this technology is constrained by its low reproducibility.^[15] Especially the complex evaporation behavior of methylammonium iodide (MAI), which includes extreme pressure rise, low rate stability, and poor adhesion to the QCM, was repeatedly reported as a challenge in several publications over the past decade.^[13,16–23] Despite these challenges, MAI is an essential precursor material for the vapor-deposition of highly efficient PSCs, as the literature overview presented in Table S1, Supporting Information illustrates.

The evaporation of MAI differs from a conventional directional evaporation process being more vapor-based was already demonstrated by Ono et al. in 2014.^[16] To determine the composition of this nondirectional evaporating MAI vapor, which is also referred to as MAI gas,^[24] mass spectrometry (MS) studies were carried out.^[22,25] Analyzing MAI by thermogravimetry coupled with MS, Juarez-Perez identified iodomethane (CH₃I) and ammonia (NH₃) as gaseous decomposition products.^[25] In contrast, the most recent study by Bækbo et al. concludes that the main decomposition products of MAI are methylamine (CH₃NH₂) and hydrogen iodide (HI).^[22] Furthermore, it is suggested that for the conversion of the lead halide both compounds (HI and CH₃NH₂) need to be present and a high chamber pressure is beneficial for a successful co-evaporation.^[22] In accordance with these findings, high deposition pressures of 10^{−4}–10^{−3} mbar, which are untypical for conventional physical

M. Roß, S. Albrecht
Department Perovskite Tandem Solar Cells
Helmholtz-Zentrum Berlin
Kekuléstraße 5, 12489 Berlin, Germany
E-mail: marcel.ross@helmholtz-berlin.de;
steve.albrecht@helmholtz-berlin.de

M. B. Stutz
Institut für Chemie
Humboldt-Universität zu Berlin
Brook-Taylor-Str. 2, 12489 Berlin, Germany
S. Albrecht
Faculty of Electrical Engineering and Computer Science
Technical University Berlin
Marchstraße 23, 10587 Berlin, Germany

 The ORCID identification number(s) for the author(s) of this article can be found under <https://doi.org/10.1002/solr.202200500>.

© 2022 The Authors. Solar RRL published by Wiley-VCH GmbH. This is an open access article under the terms of the Creative Commons Attribution License, which permits use, distribution and reproduction in any medium, provided the original work is properly cited.

DOI: 10.1002/solr.202200500

vapor depositions, have been reported.^[16,21] However, in other publications low process pressures of $\approx 10^{-6}$ mbar are described for the co-evaporation process.^[26,27]

A first indication why different reports on the pressure regime and the MAI evaporation behavior exist is given by Borchert et al., who correlate the MAI sticking on the QCM with the concentration of impurities in the precursor.^[23] They reported that large amounts of organic phosphorus compounds, which remain as impurities from the synthesis of MAI,^[28] increase the MAI adhesion to the QCM sensor and enable a better deposition rate control.^[23] However, the exact mechanism of how the impurities influence the rate measurement by QCM sensors remains open. Over the past decade, several strategies have been developed to enhance the process stability of MAI depositions for example controlling the crucible temperature or the chamber pressure, using cooled surfaces or shields, and combining different positioned QCM sensors.^[16–18,29,30] Despite these methods, the reproducibility of the MAI deposition is still limited, and the exact mechanism why the MAI evaporation can include extreme pressure rises, low rate stability, and poor as well as changing adhesion to the QCM has not been sufficiently investigated.

In this study, the evaporation, sublimation, and decomposition behavior of different MAI precursor materials in a high vacuum is analyzed by in situ mass spectrometry. We correlate the purity of commercially available MAI materials with their evaporation characteristics and identify water and methylammonium phosphite (MAH_2PO_3) as important impurities. We demonstrate that MAI with a low level of these impurities mainly decomposes into HI and CH_3NH_2 when heated in a high vacuum, whereas impure MAI directly sublimates without decomposition. We prove that these decomposition products can reunite to MAI and form perovskite in the presence of lead iodide, which makes these results essential for all co-evaporation processes involving MAI. Our findings explain why the reported deposition pressures vary between different publications and reveal why the evaporation rate of impure MAI is better traceable by QCMs. Overall, these results will assist in enhancing the reproducibility of the vacuum deposition process.

2. Results and Discussion

To identify differences in the MAI qualities, we analyzed commercially available MAI powders purchased from three different suppliers by nuclear magnetic resonance spectroscopy (^1H -NMR, ^{31}P -NMR) and determined the water content by Karl–Fisher titration (Figure 1). Based on the following analysis, we refer to them as high, medium, and low purity MAI. The exact batch numbers of each material can be found in Table 1. For all MAI powders analyzed by ^1H -NMR, the characteristic peaks of the CH_3 group at 2.6 ppm and the NH_3 group at 7.6 ppm are clearly visible (top Figure 1a–c). The largest signal at 2.5 ppm, visible in the full spectra displayed in Figure S1, Supporting Information, is associated with the deuterated dimethyl sulfoxide ($\text{DMSO}-d_6$). For the high (Figure 1a) and medium purity MAI (Figure 1b), the ^1H -NMR as well as the ^{31}P -NMR do not show additional peaks and therefore no indications for organic contamination. The low purity material includes additional peaks at 7.40, 6.69, and 6.24 ppm (Figure 1c), which belong, according to Borchert et al., to organic phosphorus

compounds, which can remain as impurities when MAI is synthesized.^[23] The fact that this contamination contains phosphorus is confirmed by the signal in the ^{31}P -NMR spectrum, which is only present for low purity MAI. It was reported that the main phosphorus impurities for MAI are methylammonium hypophosphite (MAH_2PO_2) and methylammonium phosphite (MAH_2PO_3), whereby it was demonstrated that high concentrations of MAH_2PO_2 lead to a high-field shift and high concentrations of MAH_2PO_3 lead to a signal broadening of the NH_3 group in the ^1H -NMR spectrum.^[23,28] As the peak position of the NH_3 group does not differ from that of the medium and pure material, and a significant peak broadening is present, it can be concluded that MAH_2PO_3 is the main contaminant in the low purity MAI. In addition to the NMR measurements, the water content of the MAI powders was determined by Karl–Fisher titration (Figure 1d). The high purity MAI contained the smallest amount of water with values below 700 ppm. Medium- and low purity MAI contained with average values above 1500 ppm more than the double amount of water. Based on the NMR measurements and the water content we classified the three different MAI qualities: high purity MAI—contains no MAH_2PO_3 and a low amount of water, medium purity MAI—contains no MAH_2PO_3 and a certain amount of water, and low purity MAI—contains MAH_2PO_3 and a high amount of water.

To correlate the evaporation characteristics of the different MAI qualities under high vacuum conditions, a thermal evaporation chamber equipped with a QCM was used. For each MAI quality, 0.3 g of material was weighed into a ceramic crucible and loaded into the thermal evaporator. After reaching the base pressure of 3×10^{-6} mbar in the process chamber, the crucible was heated to 130 °C and held at this constant temperature for 45 min. The process was performed for each material individually and the deposited layer thickness was recorded with the QCM for the entire time. Figure 2a shows the source temperature profile and the QCM reading for the three different MAI qualities. After 45 min the QCM sensor displays a thickness of only 25 nm for high purity MAI. For MAI with medium and low purity, the thickness reading is 140 and 200 nm, respectively, and thus significantly higher. Despite the same temperature profile being used for the three MAI powders, different amounts (mass) of the precursor material were deposited on the QCM at the same time. That the thickness on the QCM differs between the high purity (no MAH_2PO_3) and low purity (MAH_2PO_3 containing) is well in line with the publication of Borchert et al., showing a reduced adherence of high purity MAI to the QCM.^[23] Interestingly we observed a strong difference even between the high and medium purity MAI (both contain no MAH_2PO_3), which cannot be attributed to the phosphorus contamination alone. This might be caused by the different amounts of water observed in the powders. Interestingly, the temperature of the first detectable deposition rate decreases from high via medium to low purity MAI. Therefore, it is not surprising that the thickness of the deposited materials after 45 min differed. Nevertheless, the order of magnitude is striking, as the thickness of high purity MAI is reduced by a factor of eight in comparison to the low purity MAI. To understand whether this difference can be explained by the offset in evaporation temperature, the experiment was repeated but all the material in the crucible was sublimed until the rate dropped to zero and the

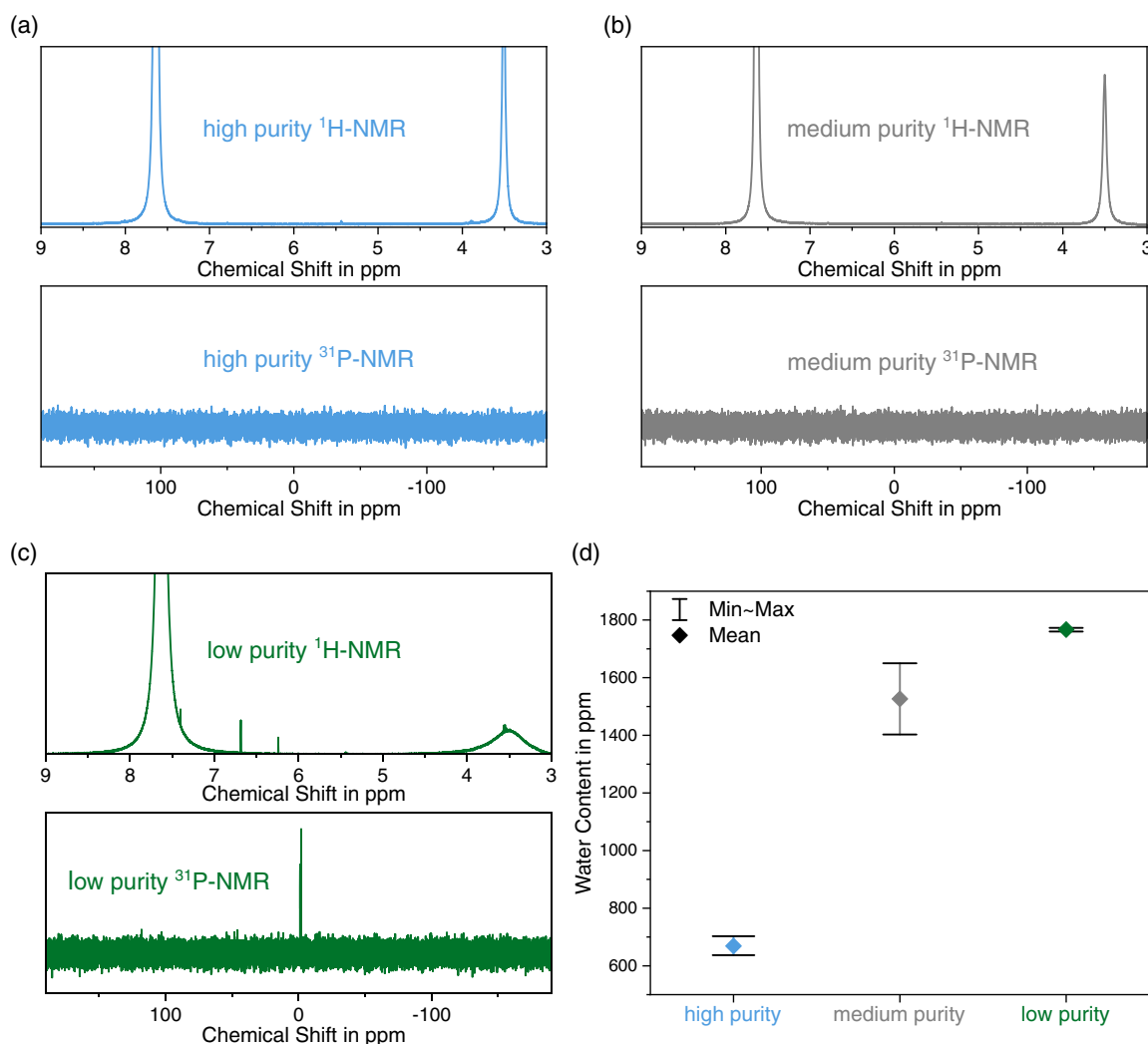


Figure 1. ^1H -NMR spectra (top) and ^{31}P -NMR spectra (bottom) measured in deuterated dimethyl sulfoxide (DMSO- D_6) for: a) high purity methylammonium iodide (MAI), b) medium purity MAI, and c) low purity MAI. d) Water content of MAI powders determined by Karl–Fisher titration. For each MAI purity, the maximum, minimum, and average water content is displayed.

Table 1. Lot numbers of MAIs from three different suppliers used for the experiments.

Supplier	Name	Lot number
Tokyo Chemical Industry	High purity	CMZ8J-FF
Sigma–Aldrich	Medium purity	MKCG0372
Luminescence Technology Corp.	Low purity	S9126-201 910 038

crucible was completely empty (only for low purity MAI a brown residue was observed in the crucible). As before, the resulting layer thickness is recorded by a QCM sensor. The deposited layer thickness on the QCM, obtained from 0.304 g MAI of each purity is displayed in Figure 2b. The results are remarkably consistent with those of the previous experiment. Significant higher thicknesses were obtained for low and medium purity MAI than for high purity MAI. The yield, i.e., the layer thickness obtained per gram of material evaporated/removed from the crucible, varies

considerably between the different MAI qualities. Overall, the trend observed for the layer thickness at the QCM correlates with the purity of the used MAI.

To gain a better understanding of how the MAI quality affects the evaporation characteristics, we further studied the material vapor using mass spectrometry. Therefore, a home build sublimation setup, displayed in Figure S2, Supporting Information, was used. This assembly consists of a glass sublimation vessel with a funnel-shaped water-cooled finger, a Pfeiffer Vacuum quadrupole mass spectrometer, an Alcatel Drytel high vacuum pumping system, and a Pfeiffer Vacuum total pressure vacuum meter. An oil bath connected to a hot plate was used as the heating source. For each of the three different MAI qualities, 0.30 g of powder was individually sublimed using similar bath temperature profiles. Due to the glass components, the sublimation can be visually monitored and photographs of the glass-ware after sublimation have been taken. We observed that the condensate films covering different areas of the setup deepened

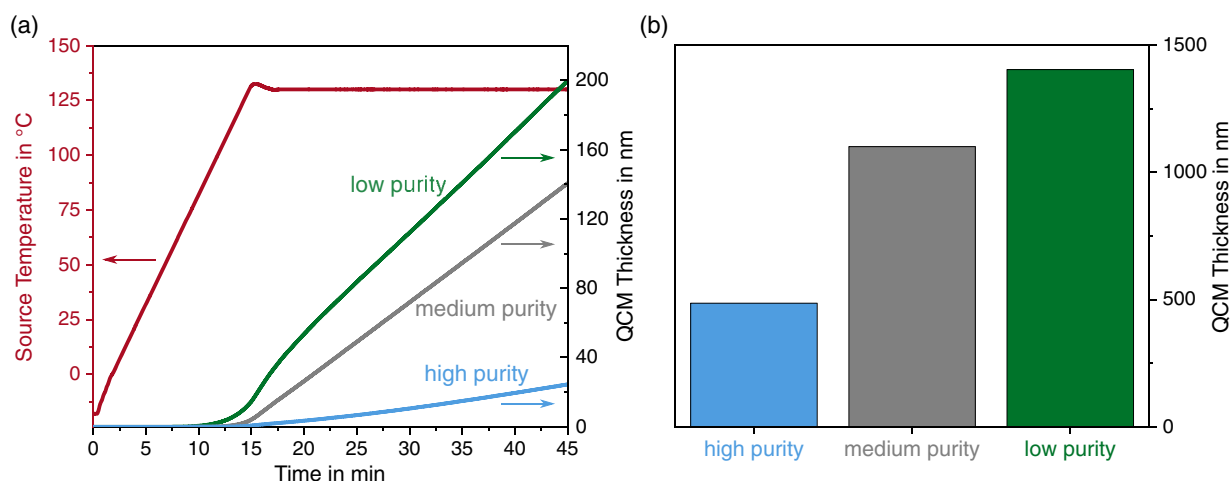


Figure 2. Layer thickness measured with the quartz crystal microbalances (QCM) sensor when: a) MAI is heated for 45 min in high vacuum and b) if 0.304 g of MAI powder is completely evaporated until the rate drops to zero. The different colors correspond to different MAI purities.

on the MAI quality used (Figure S3, Supporting Information): the low purity MAI only condensed onto the cooling finger and the lower vessel wall, in contrast, the high purity MAI was distributed throughout the entire setup. Even a 90° angle in the glassware, which excludes any direct evaporation cone (direct material flux), was no barrier. The medium purity material was as well distributed in the sublimation setup, but not to the same extent as the high purity material. The direction of the material flux seems to depend on the purity of the MAI.

Based on the decomposition products (Table S2, Supporting Information) described in the literature,^[22,25,31] the following mass to charge ratios (m/z) were monitored over the entire process: 31 (CH_3NH_2^+); 127 (I^+); 128 (HI^+); 142 (CH_3I^+). Furthermore, the total pressure and the mass to charge ratio 159, which corresponds to the molecule ion of MAI ($\text{CH}_3\text{NH}_3\text{I}^+$) were constantly measured. As no signal with m/z 159 was detected for any of the MAIs used, it is not included in Figure 3. The absence of m/z 159 means that no detectable MAI vapor was reaching the mass spectrometer, which is in line with the results reported by Bækbo et al.^[22] Figure 3a–c shows the signal of the tracked m/z values during evacuation to base pressure (with background) and heating (light red background) for the three different MAI qualities. When the high purity MAI (Figure 3a) was heated a strong increase in pressure and the m/z values of the decomposition products 31 (CH_3NH_2^+), 127 (I^+), 128 (HI^+), 142 (CH_3I^+) were clearly visible. In comparison, the pressure increase and also the m/z signals of the decomposition products were considerably lower for medium purity MAI. For low purity material (c), most of the signals were even smaller, only the signal for $m/z = 31$ did not follow this trend. The strong signal for $m/z = 31$ might be attributed to the special contamination MAH_2PO_3 found in low purity MAI. According to Levchuk et al. and Borchert et al.^[23,28] MAH_2PO_3 can decompose to H_3PO_4 at temperatures above 30 °C and form a light brown powder. This brown powder was observed as a crucible residue during the sublimation of low purity MAI (Figure S4, Supporting Information). During the decomposition of MAH_2PO_3 methylamine was released, causing the intense $m/z = 31$ signal.

As the same quantity (0.30 g) was used for all MAI qualities and the material was completely sublimed (Except for the brown residue in case of low purity MAI), the peak areas of the observed m/z ratios correlate to the amount of decomposition products formed. The direct comparison of the peak areas displayed in Figure 3d highlights that the amount of decomposition products decreases significantly from high via medium to low purity MAI. This trend is inverted to the trend in layer thicknesses on the QCM (Figure 2b) obtained in the previous experiment and to the overall amount of the impurities in water and MAH_2PO_3 present in the material.

To investigate the influence of these decomposition products on the co-evaporation process, a glass/indium tin oxide (ITO) substrate coated with about 600 nm thermally evaporated PbI_2 was placed into the sublimation setup for further experiments. The substrate was positioned at a maximum distance from the MAI source, directly at the transition point from stainless steel to glass, to ensure that there is no direct effusion path between MAI and the PbI_2 coated substrate. After the individual sublimation of all three MAI powders, the glass/ITO/ PbI_2 samples were analyzed by X-ray diffraction (XRD) and absorbance measurements. The corresponding data and a photo of each sample after sublimation are shown in Figure 4. For high purity MAI a) the substrate coated with PbI_2 has turned completely black. The absorption edge, which was 520 nm for PbI_2 and well agreed to literature values,^[32] was ≈ 770 nm after sublimation of MAI and corresponds to that of MAPbI_3 .^[33] A similar picture was obtained for the medium purity MAI b), except that the absorption edge at ≈ 770 nm was less pronounced for the converted film. For low purity MAI c), color and absorbance are unchanged compared to the pure PbI_2 reference film. The observation that with increasing amounts of decomposition products, more PbI_2 is converted into perovskites was also confirmed by XRD results displayed in Figure 4d. For high purity MAI, we observed a significant difference between the XRD pattern of the PbI_2 sample and the XRD pattern of the converted film. The reflex at 12.7°, which is typical for PbI_2 , completely vanished, instead characteristic signals for MAPbI_3 are present for example at 14.1°.^[33] Due to the decomposition products formed during MAI

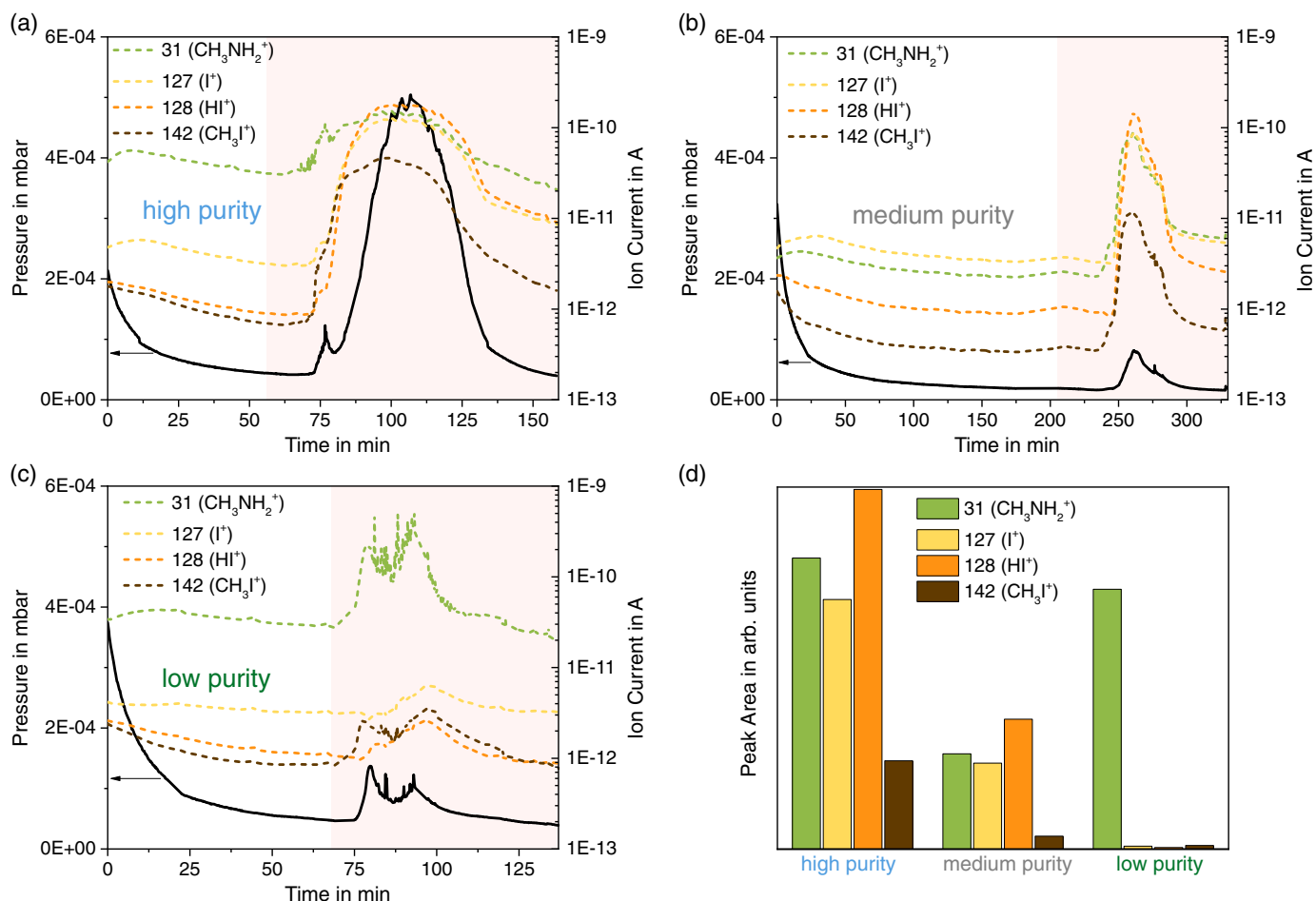


Figure 3. Mass spectrometer study for the evaporation process of 0.30 g high a), medium b), and low c) purity MAI, including evacuation phase (white background) and heating phase (light red background). Displayed are the pressure in mbar (black line corresponding to the left axes) and the ion current signals (corresponding to the right axes) observed by mass spectrometry for the monitored mass to charge values as function of time. d) Comparison of the peak areas extracted for each material.

sublimation, the 600 nm thick PbI_2 layer was almost completely converted into perovskite. For the medium purity, the intensity of the PbI_2 signal at 12.7° in the XRD pattern was still present. This indicates that the PbI_2 film was not completely converted into perovskite. For low purity MAI, the XRD pattern exhibited no indication of conversion to perovskite, only the presence of the ITO peak at 22.4° in the XRD pattern differs from the PbI_2 reference. The fact that this ITO peak was so clearly visible is most likely due to micro scratches in the PbI_2 layer, which resulted from mounting the sample into the setup. The trend observed here is in line with the overall content of impurities and the amount of observed decomposition products of MAI in mass spectrometry. The conversion of the PbI_2 layer into perovskite without a direct effusion path is, therefore, strongly connected to the presence of the MAI decomposition products. The reaction that takes place on the PbI_2 film can be understood as the reformation of the MAI and a subsequent formation of perovskite. For the synthesis of perovskites from lead iodide at normal pressure, this reaction can also be used on purpose.^[34] Overall, we observed that with increasing purity of the MAI the

thickness measured with the QCM reduces, while the amount of decomposition products and therefore the transition of the PbI_2 film to perovskite increases.

Our results indicate that MAI heated in a high vacuum can decompose or sublime, as shown in **Figure 5**. The extent of the decomposition reaction is depending on the purity of the MAI. For high purity MAI (Figure 5a) the main path is the decomposition into methylamine and hydrogen iodide. These decomposition products are at room temperature gaseous and diffuse through the setup and can reach the mass spectrometer or form solid MAI via the reverse reaction during this path. For the reverse reaction to MAI, both HI and CH_3NH_2 need to be present at the same time and place. Thus, the probability of the back reaction is rather low and the decomposition products are widely distributed in the chamber, causing the omnidirectional spread of material. As only solid MAI is detected by the QCM, the tracked rates and the final thickness are low for high purity MAI. In contrast, low purity MAI (Figure 5b) is mainly subliming without decomposition. The desublimation of gaseous MAI is a simple phase transition and can take place on every

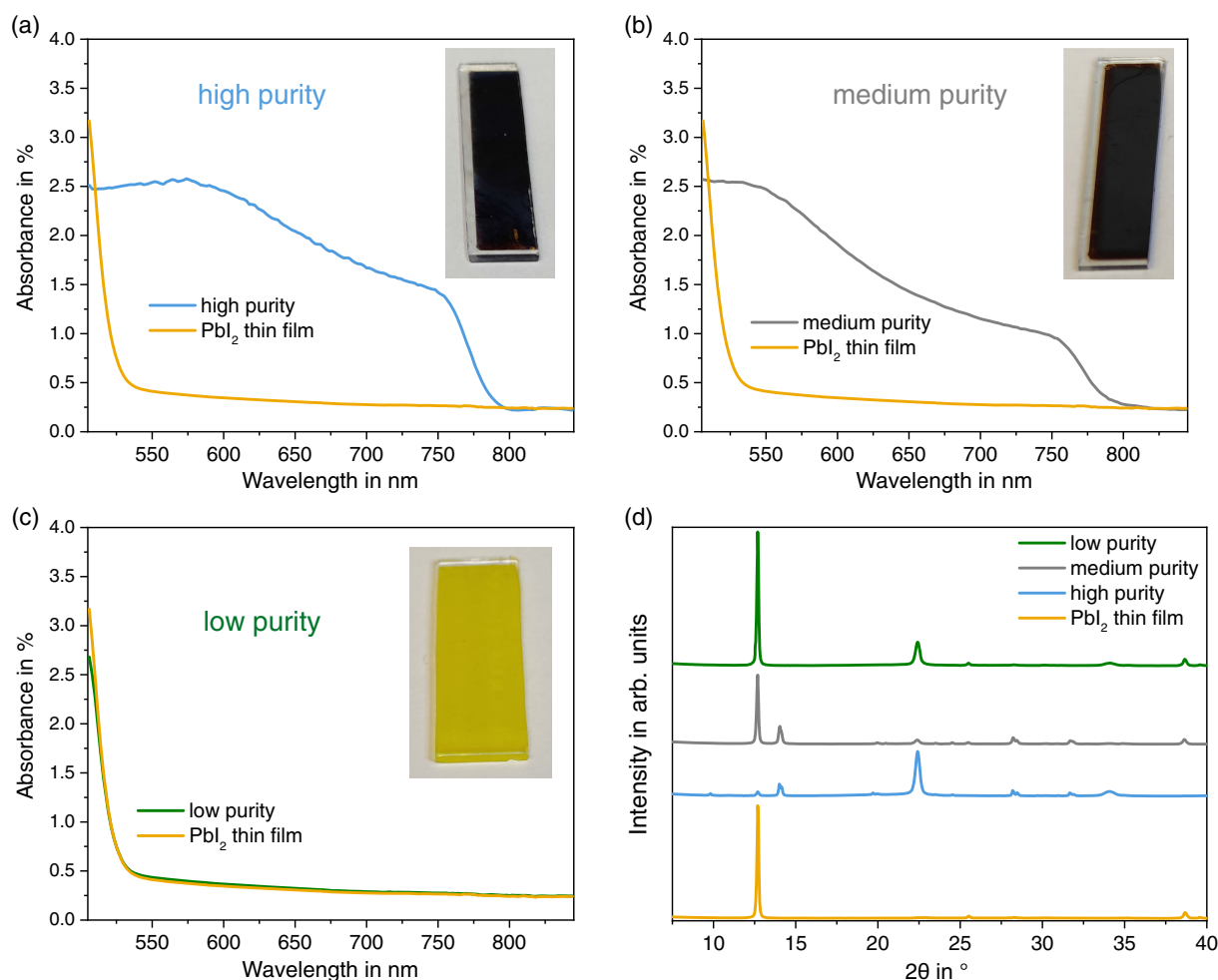


Figure 4. Absorbance spectra of PbI_2 thin films on glass/ITO before and after MAI evaporation for high a), medium b) and low c) purity MAI. In the inset of each graph, a photograph of the film after MAI evaporation is shown. d) X-ray diffraction (XRD) pattern of corresponding PbI_2 thin films on glass/ITO before and after MAI evaporation.

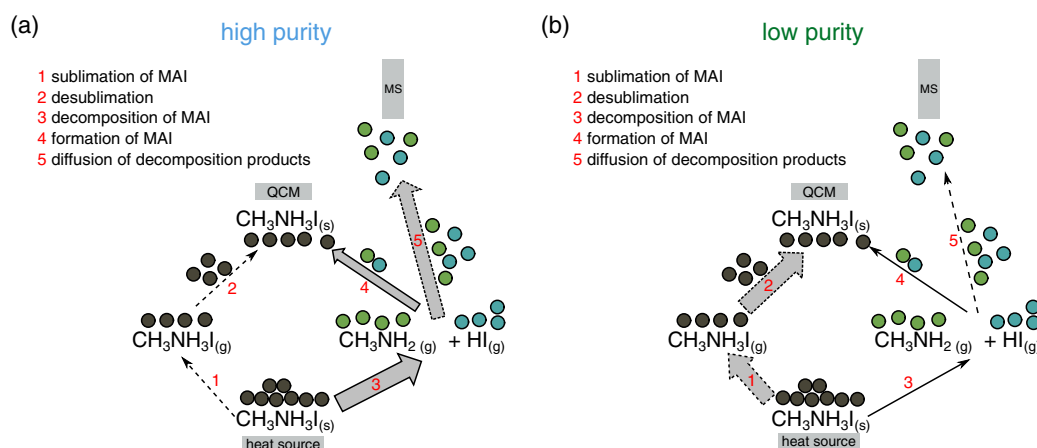


Figure 5. Schematic illustration of sublimation and decomposition processes occurring when MAI is heated in vacuum. For high purity MAI: a) the main path (indicated by thick arrows) is the decomposition into methylamine and hydrogen iodide. For low purity b) is the main path the sublimation and desublimation.

cold surface. As no decomposition products, which diffuse through the setup are formed and MAI is a solid material at room temperature, the sublimation is more directional and the detected rates, as well as the final thickness on the QCM, are much higher.

As both physical sublimation with a subsequent desublimation and chemical decomposition with a following reverse reaction can lead to solid MAI, it is difficult to distinguish these two processes. This problem is also known from other salts, e.g., ammonium chloride (NH_4Cl), which can thermally decompose into ammonia and hydrogen chloride (HCl) and can also be synthesized via the gas phase reaction of NH_3 and HCl .^[35,36] Whether the material decomposes completely when heated or if it sublimates to a certain extent is discussed in the literature.^[36–38] Interestingly, for the heating of MAI in a high vacuum the purity determines to which extent the material is transported via physical sublimation followed by desublimation or via chemical decomposition followed by a reverse reaction. To answer the question of how the impurities influence the evaporation mechanism, we will discuss two possible explanations. As the decomposition of the impurity MAH_2PO_3 leads also to the formation of methylamine, this extra amount of methylamine might shift the chemical equilibrium of the decomposition of MAI (see step 3 in Figure 5) toward molecular MAI. Also, the impurity water might change the kinetic of the decomposition reaction, for example, it was shown that water vapor can act as a catalyst for the formation of NH_4Cl from gaseous NH_3 and HCl .^[36] Both impurities could, therefore, ensure that more MAI is present in the gas phase, and explain why higher thicknesses are measured on the QCM. Besides this possibility, the impurities could also change the sublimation temperature of the MAI. If sublimation and decomposition temperature are close to each other in a high vacuum, decomposition and sublimation will compete with each other. Higher amounts of impurities might reduce intermolecular interaction in the MAI bulk and thus the energy required for sublimation. Due to the lowered sublimation temperature, the sublimation will become energetically preferable to decomposition. The intermolecular interactions influenced by impurities are plausible and studies about other salts (NaCl and KCl) indicated that impurities can increase sublimation rates and in parallel decrease the activation energies for sublimation.^[39,40] The lowering of the sublimation temperature of a material by crystal engineering is also used to avoid thermal degradation when depositing temperature-sensitive organic light-emitting diode (OLED) materials.^[41] In Figure 2, we observed that the presence of impurities (water and methylammonium phosphite) reduces the temperature of the first detected rate on the QCM.

To verify if this results from a higher sublimation temperature or is related to a better traceable rate for low purity MAI, a thermogravimetric analysis (TGA) was performed for the three different MAI qualities (Figure 6). In comparison to the experiment with the QCM shown in Figure 2, the TGA directly measures the amount of material leaving the crucible instead of the material arriving at the oscillating quartz above the source. For all three MAI qualities, the same temperature profile displayed in Figure 6 as a red line was used. The first detected mass loss (loss of about 1%) for high purity MAI is observed after 64 min. For medium and low purity MAI, this time reduces to 42 min and

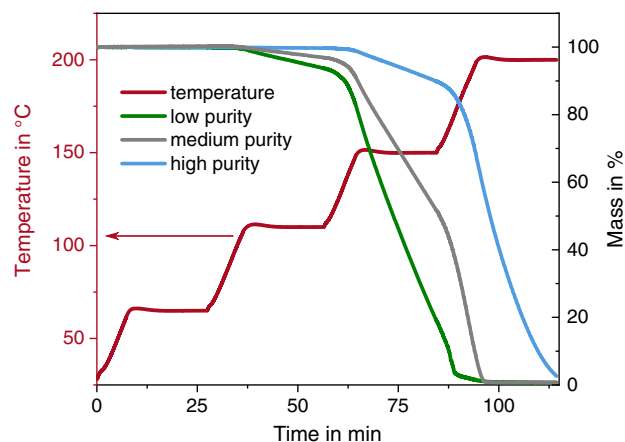


Figure 6. Thermogravimetric analysis (TGA) of MAI powders with different purities under reduced pressure. The red line corresponding to the left axes displays the used temperature profile. The right axes shows the mass of the material in the TGA crucible in percent for the three different MAI purities.

38 min, respectively. In parallel, the time and temperature needed to remove all the material from the TGA-crucible are reduced from high to low purity MAI. These results support the explanation that impurities change the sublimation temperature of the MAI material. Overall, our results suggest that decomposition and sublimation are in concurrence when MAI is heated under vacuum, therefore lowering the temperature required for sublimation by impurities favors the sublimation and thus directional evaporation of MAI. However, as the temperature needed for decomposition and sublimation are estimated to be close to each other both processes are not completely separated from each other and run in parallel. Therefore, the reaction of PbI_2 into perovskites during a co-evaporation process is potentially caused by the MAI formed via the gaseous decomposition products as well as by the direct sublimed MAI flux. How perovskites formed from decomposed MAI differ from perovskite formed via the reaction of sublimed MAI has not been investigated in detail so far. However, Borchert et al. demonstrated comparable PSCs efficiencies for pure MAI (which we found to decompose stronger) and impure MAI (which according to our findings evaporates more directly).^[23] Nevertheless, literature and our results prove that MAI powders with lower purity allow for better process control with QCMs.^[23] Our findings are particularly important for the reproducible vapor-phase deposition of highly efficient perovskite solar cells, where MAI plays a decisive role and almost all published solar cell efficiencies above 20% have been achieved using MAI-containing perovskite compositions.^[12–14,42–45]

3. Conclusion

In this work, the influence of impurities on the evaporation behavior of MAI was studied. Using nuclear magnetic resonance spectroscopy and Karl–Fisher titration, we identify water and methylammonium phosphite as important impurities in commercially available MAI powders. During thermal evaporation

experiments, we noticed a strong correlation between the evaporation characteristics of MAI and the quantity of these impurities present in the material. We demonstrated that the thickness measured with a QCM was significantly higher for low purity than for high purity MAI, although the same amount of material was removed from the crucible. Using a dedicated sublimation setup including in situ mass spectrometry, we observed a connection between MAI purity and the presents of decomposition products. With increased purity of the MAI precursor, more decomposition products have been detected during sublimation. By XRD and transmission measurements, we demonstrated that these decomposition products can interact with lead iodide and form perovskite. We proved that MAI heated in high vacuum can either undergo a sublimation with a subsequent desublimation or a chemical decomposition with a following reverse reaction leading to solid MAI in both cases. High purity MAI mainly decomposes, therefore the material is omnidirectionally distributed and the evaporation rate is hard to track by QCMs. In contrast, low purity MAI mainly sublimes which results in a directional and by QCMs observable evaporation behavior. We suggested that the impurities reduce the sublimation temperature of MAI, which means that sublimation becomes energetically preferable to decomposition. Our results reveal why for the deposition of MAI extreme chamber pressure rise, low rate-stability over time, and poor adhesion to the QCM have been constantly described as problems in the literature. Furthermore, the insights about the influence of impurities can serve as a guideline for the precursor material selection and will help to increase the reproducibility of the evaporation process.

4. Experimental Section

A CreaPhys “PEROvap” thermal evaporation tool integrated into a glove box (MBraun) filled with nitrogen atmosphere was used for the evaporation experiments. The temperature of the inner shielding, which is surrounding all evaporation sources and passively cools the QCM, was set to -25°C for all processes. For the preparation of the lead iodide films, PbI_2 (99.99%, trace metals basis) from TCI and ITO substrates purchased from Automatic Research GmbH were used. The suppliers and lot numbers of the MAI powders used for the experiments are displayed in Table 1.

For absorbance measurements, a PerkinElmer Lambda—1050 UV/VIS/NIR double beam spectrophotometer with an integrating sphere was used.

XRD patterns were recorded with a Bruker D8 diffractometer in Bragg–Brentano geometry. For all measurements, the Cu K-alpha radiation emitted from an X-ray tube operated at 40 mA and 40 kV acceleration voltage was used.

^1H -NMR and ^{31}P -NMR spectra were recorded on an Avance II 500 (^1H : 500 MHz, ^{31}P : 202 MHz) spectrometer from Bruker. The measurements were carried out at room temperature. The DMSO- d_6 was purchased from Deutero. The residual proton signal of the deuterated solvent ($\delta = 2.50$ ppm) was used as an internal reference for ^1H -NMR experiments.

The mass spectrometry experiments were performed using a home-built setup, which consists of a glass sublimation vessel with a funnel-shaped water-cooled finger, an Alcatel Drytel high vacuum pumping system, and a Pfeiffer Vacuum total pressure vacuum meter. The Pfeiffer Prisma QMS 200F quadrupole mass spectrometer is equipped with a Faraday detector. All measurements were controlled with the Quadstar 32-bit software. A voltage of 70 V was used for the cathode of the ion source. After each experiment, the filament was cleaned using the auto degas function.

The water content of the MAI powders was determined by Karl–Fisher titration. The method is based on the reaction of sulfur dioxide with iodine, which only takes place in the presence of water and is a standard analytical method for water determination.^[46] The measurements have been carried out as a contract analysis in the external laboratory “ASG Analytik-Service AG.”

TGA was performed with a TG 209 F1 Iris system coupled with a QMS 403 Aëolos Quadro from Netzsch. The measurements and the analysis was done using the Proteus software. For all experiments, 85 μL open Al_2O_3 ceramic crucibles filled with about 30 mg MAI powder were used. For the baseline correction, a clean and empty crucible of the same fabricate was used. The experiments were performed with the option “vacuum on during measurement” leading to a pressure lower than 1×10^{-2} mbar.

Supporting Information

Supporting Information is available from the Wiley Online Library or from the author.

Acknowledgements

For technical assistance, the authors thank T. Lußky, H. Heinz, C. Ferber, (Institute for Silicon Photovoltaics), and C. Leistner (Institute Applied Materials). The authors acknowledge funding from the Federal Ministry of Education and Research (BMBF) for funding of the Young Investigator Group Perovskite Tandem Solar Cells within the program “Materialforschung für die Energiewende” (Grant no. 03SF0540), the Helmholtz Association within the HySPRINT Innovation lab project, and the HyPerCells joint Graduate School. The authors thank I. Lauerhmann (PVComB) for providing the mass spectrometer.

Open Access funding enabled and organized by Projekt DEAL.

Conflict of Interest

The authors declare no conflict of interest.

Data Availability Statement

The data that support the findings of this study are available from the corresponding author upon reasonable request.

Keywords

co-evaporation, impurities, methylammonium iodide, perovskites, reproducibility, vapor-phase deposition

Received: June 2, 2022

Revised: July 8, 2022

Published online: August 7, 2022

- [1] S. De Wolf, J. Holovsky, S.-J. Moon, P. Löper, B. Niesen, M. Ledinsky, F.-J. Haug, J.-H. Yum, C. Ballif, *J. Phys. Chem. Lett.* **2014**, *5*, 1035.
- [2] J. Huang, Y. Yuan, Y. Shao, Y. Yan, *Nat. Rev. Mater.* **2017**, *7*, 17042.
- [3] K. X. Steirer, P. Schulz, G. Teeter, V. Stvanovic, M. Yang, K. Zhu, J. J. Berry, *ACS Energy Lett.* **2016**, *1*, 360.
- [4] T. Soto-Montero, W. Soltanpoor, M. Morales-Masis, *APL Mater.* **2020**, *8*, 110903.
- [5] J. J. Yoo, G. Seo, M. R. Chua, T. G. Park, Y. Lu, F. Rotermund, Y.-K. Kim, C. S. Moon, N. J. Jeon, J.-P. Correa-Baena, V. Bulovic, S. S. Shin, M. G. Bawendi, J. Seo, *Nature* **2021**, *590*, 7847.

- [6] NREL, Best Research-Cell Efficiency Chart, **2022**, <https://www.nrel.gov/pv/cell-efficiency.html> (accessed: May 2022).
- [7] L. K. Ono, M. R. Leyden, S. Wang, Y. Qi, *J. Mater. Chem. A* **2016**, *4*, 6693.
- [8] J.-P. Correa-Baena, A. Abate, M. Saliba, W. Tress, T. J. Jacobsson, M. Grätzel, A. Hagfeldt, *Energy Environ. Sci.* **2017**, *10*, 710.
- [9] C. Momblona, O. Malinkiewicz, C. Roldan-Carmona, A. Soriano, L. Gil-Escrig, E. Bandiello, M. Scheepers, E. Edri, H. J. Bolink, *APL Mater.* **2014**, *2*, 7.
- [10] G. Sauerbrey, *Z. Phys.* **1959**, *155*, 206.
- [11] M. Liu, M. B. Johnston, H. J. Snaith, *Nature* **2013**, *501*, 7467.
- [12] C. Momblona, L. Gil-Escrig, E. Bandiello, E. M. Hutter, M. Sessolo, K. Lederer, J. Blochwitz-Nimoth, H. J. Bolink, *Energy Environ. Sci.* **2016**, *9*, 3456.
- [13] J. Li, H. Wang, X. Y. Chin, H. A. Dewi, K. Vergeer, T. W. Goh, J. W. M. Lim, J. H. Lew, K. P. Loh, C. Soci, T. C. Sum, H. J. Bolink, N. Mathews, S. Mhaisalkar, A. Bruno, *Joule* **2020**, *4*, 1035.
- [14] D. Perez-del Rey, P. P. Boix, M. Sessolo, A. Hadipour, H. J. Bolink, *J. Phys. Chem. Lett.* **2018**, *9*, 1041.
- [15] Y. Vaynzof, *Adv. Energy Mater.* **2020**, *48*, 2003073.
- [16] L. K. Ono, S. Wang, Y. Kato, S. R. Raga, Y. Qi, *Energy Environ. Sci.* **2014**, *7*, 3989.
- [17] O. Malinkiewicz, A. Yella, Y. H. Lee, G. M. Espallargas, M. Graetzel, M. K. Nazeeruddin, H. J. Bolink, *Nat. Photonics* **2014**, *8*, 128.
- [18] J. Teuscher, A. Ulianov, O. Müntener, M. Grätzel, N. Tétreault, *ChemSusChem* **2015**, *8*, 3847.
- [19] D. Yang, Z. Yang, W. Qin, Y. Zhang, S. Liu, C. Li, *J. Mater. Chem. A* **2015**, *3*, 9401.
- [20] D. Zhao, W. Ke, C. R. Grice, A. J. Cimaroli, X. Tan, M. Yang, R. W. Collins, H. Zhang, K. Zhu, Y. Yan, *Nano Energy* **2016**, *19*, 88.
- [21] S. Olthof, K. Meerholz, *Sci. Rep.* **2017**, *7*, 40267.
- [22] M. J. Bækbo, O. Hansen, I. Chorkendorff, P. C. K. Vesborg, *RSC Adv.* **2018**, *8*, 29899.
- [23] J. Borchert, I. Leychuk, L. C. Snoek, M. U. Rothmann, R. Haver, H. J. Snaith, C. J. Brabec, L. M. Herz, M. B. Johnston, *ACS Appl. Mater. Interfaces* **2019**, *11*, 28851.
- [24] C. Wittich, E. Mankel, O. Clemens, K. Lakus-Wollny, T. Mayer, W. Jaegermann, H.-J. Kleebe, *Thin Solid Films* **2018**, *650*, 51.
- [25] E. J. Juarez-Perez, Z. Hawash, S. R. Raga, L. K. Ono, Y. Qi, *Energy Environ. Sci.* **2016**, *9*, 3406.
- [26] J. B. Patel, J. Wong-Leung, S. Van Reenen, N. Sakai, J. T. W. Wang, E. S. Parrott, M. Liu, H. J. Snaith, L. M. Herz, M. B. Johnston, *Adv. Electron. Mater.* **2017**, *3*, 1600470.
- [27] T. Gallet, R. G. Poeria, E. M. Lanzoni, T. Abzieher, U. W. Paetzold, A. Redinger, *ACS Appl. Mater. Interfaces* **2021**, *13*, 2642.
- [28] I. Levchuk, Y. Hou, M. Gruber, M. Brandl, P. Herre, X. Tang, F. Hoegl, M. Batentschuk, A. Osvet, R. Hock, W. Peukert, R. R. Tykewinski, C. J. Brabec, *Adv. Mater. Interfaces* **2016**, *3*, 1600593.
- [29] B.-S. Kim, L. Gil-Escrig, M. Sessolo, H. J. Bolink, *J. Phys. Chem. Lett.* **2020**, *11*, 6852.
- [30] R. Kottokaran, H. A. Gaonkar, H. A. Abbas, M. Noack, V. Dalal, *J. Mater. Sci. Mater. Electron* **2019**, *30*, 5487.
- [31] D. P. Nenon, J. A. Christians, L. M. Wheeler, J. L. Blackburn, E. M. Sanehira, B. Dou, M. L. Olsen, K. Zhu, J. J. Berry, J. M. Luther, *Energy Environ. Sci.* **2016**, *9*, 2072.
- [32] Z. Y. Wu, B.-L. Jian, H.-C. Hsu, *Opt. Mater. Express* **2019**, *9*, 1882.
- [33] F. Palazon, D. Pérez-del Rey, B. Dänekamp, C. Dreessen, M. Sessolo, P. P. Boix, H. J. Bolink, *Adv. Mater.* **2019**, *31*, 1902692.
- [34] S. R. Raga, L. K. Ono, Y. Qi, *J. Mater. Chem. A* **2016**, *4*, 2494.
- [35] R. D. Schultz, A. O. Dekker, *J. Phys. Chem.* **1956**, *60*, 1095.
- [36] C. M. Banic, J. V. Iribarne, *J. Geophys. Res.* **1980**, *85*, 7459.
- [37] R. S. Zhu, J. H. Wang, M. C. Lin, *J. Phys. Chem. C* **2007**, *111*, 13831.
- [38] P. Goldfinger, G. Verhaegen, *J. Chem. Phys.* **1969**, *50*, 1467.
- [39] C. Grimes, J. Hinkley, J. E. Lester, *J. Chem. Phys.* **1972**, *56*, 524.
- [40] R. H. Wagoner, J. P. Hirth, *J. Chem. Phys.* **1977**, *67*, 3074.
- [41] T. Lee, M. S. Lin, *Cryst. Growth Des.* **2007**, *7*, 1803.
- [42] M. Roß, L. Gil-Escrig, A. Al-Ashouri, P. Tockhorn, M. Jošt, B. Rech, S. Albrecht, *ACS Appl. Mater. Interfaces* **2020**, *12*, 39261.
- [43] Y. Choi, D. Koo, G. Jeong, U. Kim, H. Kim, F. Huang, H. Park, *Energy Environ. Sci.* **2022**.
- [44] M. M. Tavakoli, P. Yadav, D. Prochowicz, R. Tavakoli, *Sol. RRL* **2021**, *5*, 2000552.
- [45] M. Roß, S. Severin, M. B. Stutz, P. Wagner, H. Köbler, M. Favin-Lévêque, A. Al-Ashouri, P. Korb, P. Tockhorn, A. Abate, B. Stannowski, B. Rech, S. Albrecht, *Adv. Energy Mater.* **2021**, 2101460.
- [46] E. Scholz, In H. Günzler, R. Borsdorf, W. Fresenius, W. Huber, H. Kelker, I. Lüderwald, *Analytiker-Taschenbuch* (Eds: G. Tölg, H. Wisser), Springer Berlin, Heidelberg **1990**, p. 271.